Available online at www.sciencedirect.com

ScienceDirect

Ceramics International 40 (2014) 2281–2286

CERAMICS INTERNATIONAL

www.elsevier.com/locate/ceramint

# Effects of (Dy, Zn) co-doping on structural and electrical properties of $BiFeO_3$ thin films

C.M. Raghavan, J.W. Kim, S.S. Kim*

*Department of Physics, Changwon National University, Changwon, Gyeongnam 641-773, Republic of Korea*

Received 1 July 2013; received in revised form 30 July 2013; accepted 30 July 2013
Available online 6 August 2013

**Abstract**

Pure $BiFeO_3$ (BFO) and (Dy, Zn) co-doped $(Bi_{0.9}Dy_{0.1})(Fe_{0.975}Zn_{0.025})O_{3-\delta}$ (BDFZO) thin films were prepared on Pt(111)/Ti/$SiO_2$/Si(100) substrates by a chemical solution deposition method. Effects of (Dy, Zn) co-doping on the structural and electrical properties of BFO were studied. Both the thin films were crystallized as randomly oriented polycrystalline distorted rhombohedral structures, with no detectable impurity and secondary phases. Large remnant polarization ($2P_r$) of 47 μC/cm$^2$, low coercive electric field ($2E_c$) of 925 kV/cm at 1143 kV/cm and low leakage current density of $1.30\times10^{-6}$ A/cm$^2$ at 100 kV were measured for the BDFZO thin film. The improved electrical properties of the BDFZO thin film are ascribed to the stabilization of perovskite structure, defect complex formation between acceptors $Zn^{2+}$ and oxygen vacancies of $[(Zn^{2+}_{Fe^{3+}})'-(V^{\bullet\bullet}_{O^{2-}})]$, pronounced off-center displacement in the perovskite and structural distortion by the Dy and Zn ions doping.


*Keywords:* A. Films; C. Electrical properties; C. Ferroelectric properties; D. Perovskites

## 1. Introduction

Perovskite bismuth ferrite $BiFeO_3$ (BFO) has emerged as a very promising candidate for the multiferroic applications. In BFO, the ferroelectric properties occur below Curie temperature $T_C=1100$ K due to charge ordering caused by the ordering of lone electron pairs of $Bi^{3+}$ ions. The magnetic properties with weak ferromagnetic moment result from the complex ordering of $Fe^{3+}$ spins and they occur below the Néel temperature $T_N=643$ K. Both the ferroelectric and the ferromagnetic transitions occur above room temperature in the perovskite BFO [1–3]. Therefore, it has been considered as superior among the existed multiferroic materials. Theoretical studies revealed large remnant polarization ($>90$ μC/cm$^2$) in thin film BFO rather than bulk [4]. The large polarization observed in the thin film is mainly attributed to the small changes in the lattice parameter caused by the lattice strain [4,5].

It is technologically important to improve electrical and ferroelectric properties of the perovskite BFO to completely overcome the toxic lead based lead zirconium titanate in ferroelectric devices [5]. Presence of oxygen vacancies, nucleation of parasitic phases at grain boundaries and interfaces, $Fe^{2+}/Fe^{3+}$ valence fluctuation and poor microstructure are the crucial factors for the large electrical leakage in the ferroelectric BFO [2,6–8]. There are flurry of ongoing researches to control the electrical leakage via different approaches. Among them, the cationic substitution into Bi- and Fe-sites of the BFO using rare earth (*RE*) and transition metal ions is strongly recommended for the effective reduction of leakage current density and the improvement of ferroelectric polarization [8–15]. The doping elements are also reported to alter the cycloid spin structure which in turn enhance the magnetization of the BFO [16]. Recently, Hu et al. observed improved electrical and ferroelectric properties for the Ti and Zn doped BFO thin film fabricated by a sol–gel based metal organic decomposition method [17]. The formation of defect complexes between cationic acceptors and oxygen vacancies plays a vital role in the improvements of electrical and ferroelectric properties of the Ti and Zn doped BFO thin film [17]. Rare earth ions with relatively low electronegativity compared to oxygen have strong influence on the ferroelectric and ferromagnetic properties of the

*Corresponding author. Tel.: +82 552133421; fax: +82 552670264.
*E-mail address:* sskim@changwon.ac.kr (S.S. Kim).

0272-8842/$ - see front matter © 2013 Elsevier Ltd and Techna Group S.r.l. All rights reserved.
http://dx.doi.org/10.1016/j.ceramint.2013.07.148

BFO [10]. The electronegativity of Dy (1.22) is lower than that of the oxygen (3.44). And the ionic radius of $Dy^{3+}$ (1.25 Å) is smaller than that of $Bi^{3+}$ (1.45 Å). Hence, substitution of Dy ion into Bi site is relatively easy.

Recently, the improved magnetic properties were reported for the Dy doped BFO [18]. However, the doping of $Dy^{3+}$ ion weakens the stereochemical activity of the $Bi^{3+}$ ion $6s^2$ lone pair electrons, which will degrade the ferroelectric polarization of the material [18,19]. For potential multiferroic applications, it is essential to observe strong ferroelectric and ferromagnetic properties, simultaneously. Therefore, in this study, the Zn ion is co-doped for the further improvement of ferroelectric properties. Moreover, addition of divalent $Zn^{2+}$ ion into BFO could able to form strong defect complex, such as $[(Zn^{2+}_{Fe^{3+}})'-(V^{\bullet\bullet}_{O^{2-}})]$. The formation of defect complex enhances the ferroelectric remnant polarization [17]. The detail studies on structural, electrical and ferroelectric properties of the (Dy, Zn) co-doped $(Bi_{0.9}Dy_{0.1})(Fe_{0.975}Zn_{0.025})O_{3-\delta}$ thin film are discussed in detail.

## 2. Experimental procedure

The raw materials used for the precursor solutions are bismuth nitrate pentahydrate ($Bi(NO_3)_3 \cdot 5H_2O$), iron nitrate nonahydrate ($Fe(NO_3)_3 \cdot 9H_2O$), dysprosium nitrate pentahydrate ($Dy(NO_3)_3 \cdot 5H_2O$) and zinc nitrate hexahydrate ($Zn(NO_3)_3 \cdot 6H_2O$). Ethylene glycol ($OH(CH_2)_2OH$) and 2-methoxyethanol ($CH_3O(CH_2)_2OH$) were mixed at 40 °C in a water bath for 30 min and used as a solvent. Bismuth nitrate pentahydrate (5 mol% excess), acetic acid ($CH_3CO_2H$) (as a catalyst) and iron nitrate nonahydrate were added sequentially into the mixed solvent with 30 min stirring intervals at room temperature to form a BFO precursor solution. For the (Dy, Zn) co-doping, before the addition of the iron nitrate pentahydrate, dysprosium nitrate pentahydrate and zinc nitrate hexahydrate were added with 30 min stirring intervals. Finally, iron nitrate nonahydrate was added to form a BDFZO precursor solution. The final solutions of the BFO and the BDFZO were stirred for 3 h at room temperature for the homogenization. The concentrations of all precursor solutions were adjusted to 0.1 M.

The BFO and the BDFZO precursor solutions were spin coated on Pt(111)/Ti/$SiO_2$/Si(100) substrates at a constant spinning rate of 3000 rpm for 20 s. The spin coated wet thin films were prebaked at 360 °C for 10 min on a hot plate to eliminate organic moieties. The coating and the prebaking processes were repeated 12 times to obtain the desired film thickness. Finally, the thin films were subjected to conventional annealing at 550 °C for 30 min under a nitrogen atmosphere for crystallization. Platinum electrodes with areas of $1.54 \times 10^{-4}$ $cm^2$ were deposited on the top surfaces of the thin films by ion sputtering through a metal shadow mask to form a capacitor structure.

The structures of the BFO and the BDFZO thin films were investigated by an X-ray diffractometer (Rigaku, MiniFlex II) and a Raman spectroscope (Jasco, NRS-3100). The surface morphologies and film thicknesses of the thin films were examined by a field emission scanning electron microscope (Tescan, MIRA II LMH). The ferroelectric hysteresis loops of the thin films were measured at a frequency of 10 kHz with triangular pulses by a standardized ferroelectric test system (Modified Sawyer–Tower circuit with oscilloscope). The electrical properties, such as leakage current density and dielectric property, of the thin films were measured by an electrometer (Keithley, 6517 A) and a low frequency impedance analyzer (HP, 4192 A), respectively.

## 3. Results and discussion

Fig. 1(a) shows X-ray diffraction (XRD) patterns of the BFO and the BDFZO thin films deposited on Pt(111)/Ti/$SiO_2$/Si(100) substrates. As shown in Fig. 1(a), both the thin films were indexed for the randomly oriented polycrystalline of distorted rhombohedral structure with *R3c* space group [JCPDS no: 72-2035]. Formations of the pure perovskite phases were confirmed by the absence of additional peaks corresponding to the secondary or impurity phases in both the samples. However, as shown in Figs. 1(b) and (c), small changes in the diffraction patterns corresponding to (100) and (110/1$\bar{1}$0) planes were observed for the BFO and the BDFZO thin films. As shown in Fig. 1(b), small higher angle shift in the vicinity of the 22.5° was observed in the BDFZO thin film and this shift is not significant to change the original perovskite structure. From Fig. 1(c), overlapping of split peaks corresponding (110/1$\bar{1}$0) planes in the vicinity of 32° was clearly observed for the BDFZO. However, the Lorentz fitting showed the existence of the split in the BDFZO thin film. These results indicate that the internal stress induced by the doping elements leads to the distortion in perovskite without changing the original structure [20,21].

Raman scattering spectra for the BFO and the BDFZO thin films measured at room temperature are shown in Fig. 2. For the rhombohedrally distorted *R*3c space group, 13 ($4A_1$+9*E*) active Raman modes were predicted. All of the Raman modes observed in the BFO and the BDFZO thin films are well

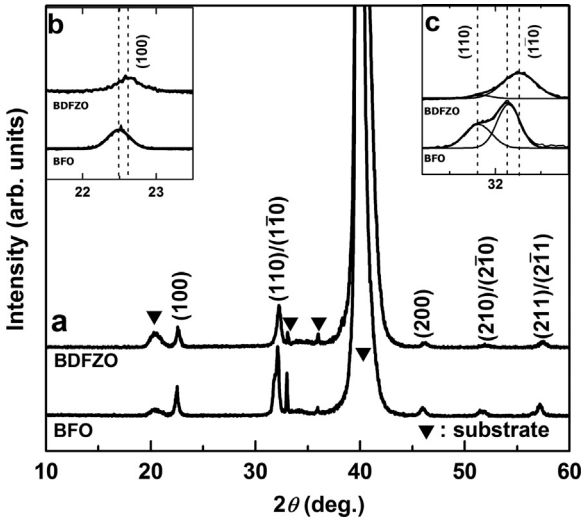


Fig. 1. (a) XRD patterns of the BFO and the BDFZO thin films deposited on Pt(111)/Ti/$SiO_2$/Si(100) substrates. Magnified XRD patterns with Lorentz fitted curves in the vicinities of (b) $2\theta=22°$ corresponding to (100) and (c) $2\theta=32.0°$ corresponding to (110)/(1$\bar{1}$0) planes.

correlated with those for the rhombohedrally distorted (*R*3*c*) perovskite structure [3,22]. The exact peak positions have been obtained by fitting the measured spectra and decomposing the fitted curves into individual Lorentz components. According to the group theory, the $A_1$ phonon modes observed in the low frequency region are attributed to the Bi–O vibration and the high frequency *E* modes are related to the Fe–O vibration [22]. On comparing the $Bi^{3+}$ ionic radius (1.45 Å) with twelve coordination, the $Dy^{3+}$ ionic radius (1.25 Å) is smaller. Hence, it is easy to substitute Dy into the Bi site of the BFO. The changes observed in the low frequency Raman modes for the BDFZO thin film are mainly attributed to the Dy substitution into the Bi site of the perovskite BFO. The Dy substitution leads to the distortion in Bi–O bonding, which in turn broadened the low frequency $A_1$ modes of the BDFZO thin film as shown in Fig. 2 [23,24]. The electronegativity of Dy (1.22) is lower than those of O (3.44) and Bi (2.02). Hence, the electronegativity difference Dy–O is higher than that of Bi–O, which in turn strengthens the Bi(*RE*)–O covalent bond and induces a more pronounced off-center displacement in the BFO [10,23]. The smaller ionic radius of the Dy and relative

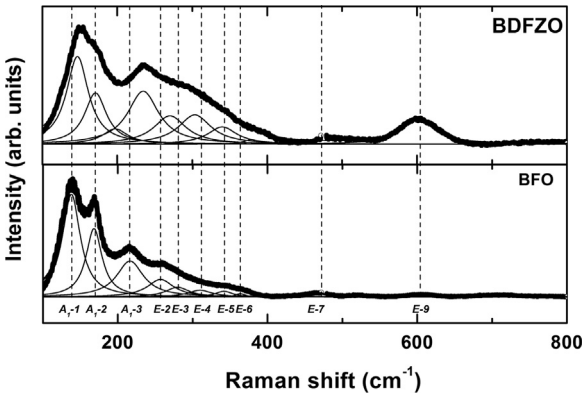


Fig. 2. Raman scattering spectra with fitted curves (thick solid lines) and the decomposed active modes (thin solid lines) of the BFO and the BDFZO thin films.

Table 1
Comparison of the observed Raman frequencies of the BFO and the BDFO thin films.

| Raman modes | | | | | | | | | | | | |
|---|---|---|---|---|---|---|---|---|---|---|---|---|
| | $A_1$-1 | $A_1$-2 | $A_1$-3 | *E*-2 | *E*-3 | *E*-4 | *E*-5 | *E*-6 | $A_1$-4 | *E*-7 | *E*-8 | *E*-9 |
| BFO | 137 | 168 | 216 | 257 | 279 | 309 | 341 | 363 | – | 467 | – | – |
| BDFZO | 146 | 170 | 197 | 234 | 270 | 303 | 340 | 378 | – | – | – | 601 |

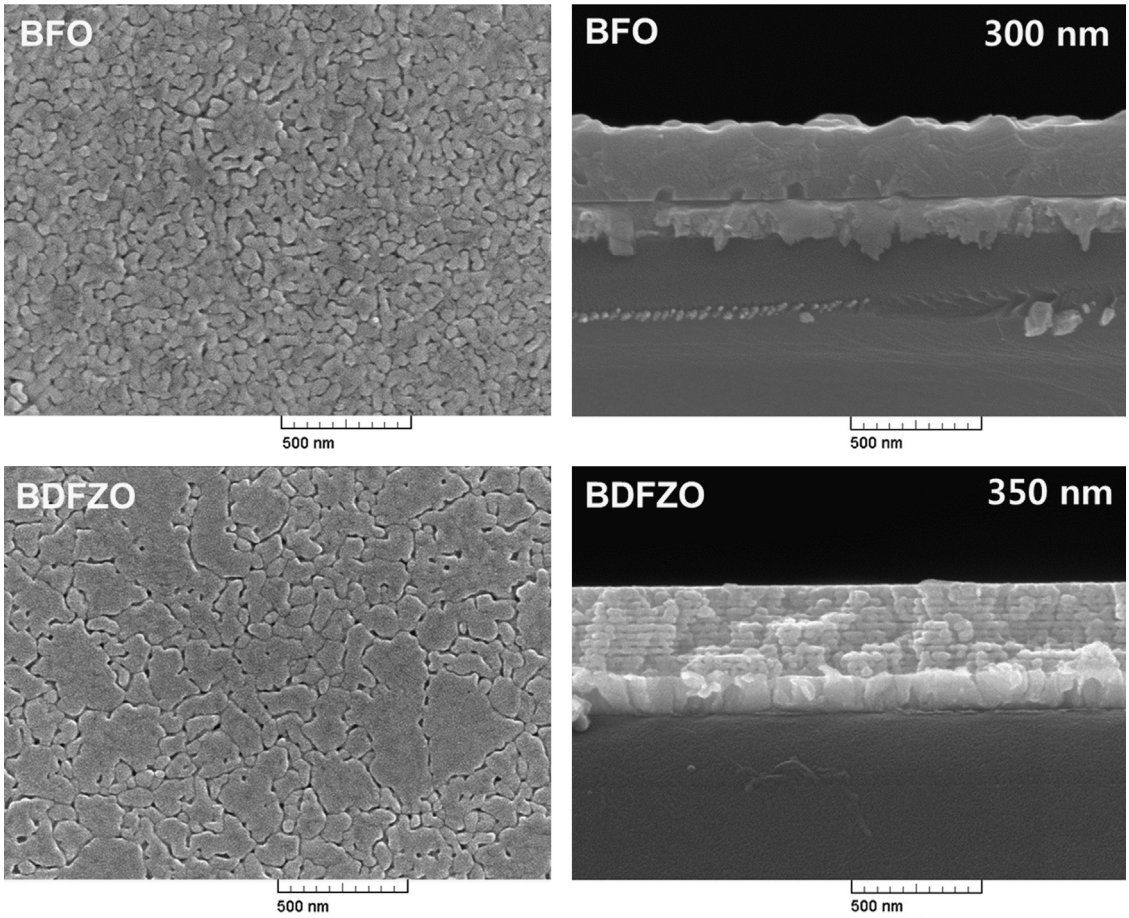


Fig. 3. SEM images of the surface morphologies and the cross-sectional views of the BFO and the BDFZO thin films.

electronegativity difference between Dy–O and Bi–O should have influence on the Raman scattering spectrum of the BDFZO at low electric field region [23]. As compared to the $Dy^{3+}$ ion, the $Zn^{2+}$ ion has less significant effect on the Raman scattering spectrum. For the comparisons, the Raman modes for the BFO and BDFZO are given in Table 1. In the high frequencies for the BDFZO thin film, there are some peaks disappearing which might be related to $Zn^{2+}$ on the Fe-site of the BFO.

The surface morphological features of the BFO and the BDFZO thin films are shown in Fig. 3. The changes in microstructures were clearly observed between the BFO and the BDFZO thin films, which indicate the influence of co-doping elements on the nucleation of the BFO thin films. Dense grain distribution with micro-pores was observed in the BFO thin film. While, inhomogeneous grain clustering was observed in the BDFZO thin film. The surface of the BDFZO thin film is smoother compared to the BFO thin film. The Dy–O bond energy is higher than that of the Bi–O bond energy, which results more heat release during film growth in turn stabilizes the structure to maintain the smooth surface [10]. The thicknesses of the BFO and the BDFZO thin films were approximately 300 and 350 nm from the cross-sectional SEM images.

Variations of the leakage current densities ($J$) as functions of applied electric fields ($E$) for the BFO and the BDFZO thin films are shown in Fig. 4(a). The BDFZO thin film showed low order of leakage current densities compared to the BFO thin film. The measured $J$ values of the BFO and the BDFZO thin films were $2.58 \times 10^{-2}$ A/cm$^2$ and $1.30 \times 10^{-6}$ A/cm$^2$ at an applied electric field of 100 kV/cm, respectively. The $J$ value of the BDFZO thin film was about four orders lower than that of the BFO thin film. It is believed that there are two major factors for the conduction in BFO, such as presence of oxygen vacancies and valence fluctuation ($Fe^{2+}/Fe^{3+}$) caused by the electronically unstable Fe ion. The decrease of $J$ value for the BDFZO thin film indicates reduction of oxygen vacancies and stabilization of the perovskite structure by doping of the Dy and Zn ions [6,14]. The bond strength of the Dy–O (615 kJ/mol) is larger than that of the Bi–O (337.2 kJ/mol) bond strength. Therefore, doping of the rare earth Dy ion into the Bi-site could control the volatilization of the Bi ion, which in turn stabilizes the perovskite phase of the BFO [14,25]. Addition of the divalent $Zn^{2+}$ ion is reported to facilitate the formation of the defect complexes between $Zn^{2+}$ and oxygen vacancies as $[(Zn^{2+}_{Fe^{3+}})'-(V^{\bullet\bullet}_{O^{2-}})]$ [17]. In perovskite BFO, the mobile oxygen vacancies act as donor like trapping center for electrons. The energy level of the oxygen vacancies is very close to the conduction band of the BFO. Hence, the electrons could be easily promoted for the conduction with respect to the applied electric field. However, the formation of the $[(Zn^{2+}_{Fe^{3+}})'-(V^{\bullet\bullet}_{O^{2-}})]$ defect complex required large electric field to break and avail electrons to be free for the conduction [17]. Formation of the grain clusters might also play a role in the reduction of leakage current of the co-doped BDFZO thin film.

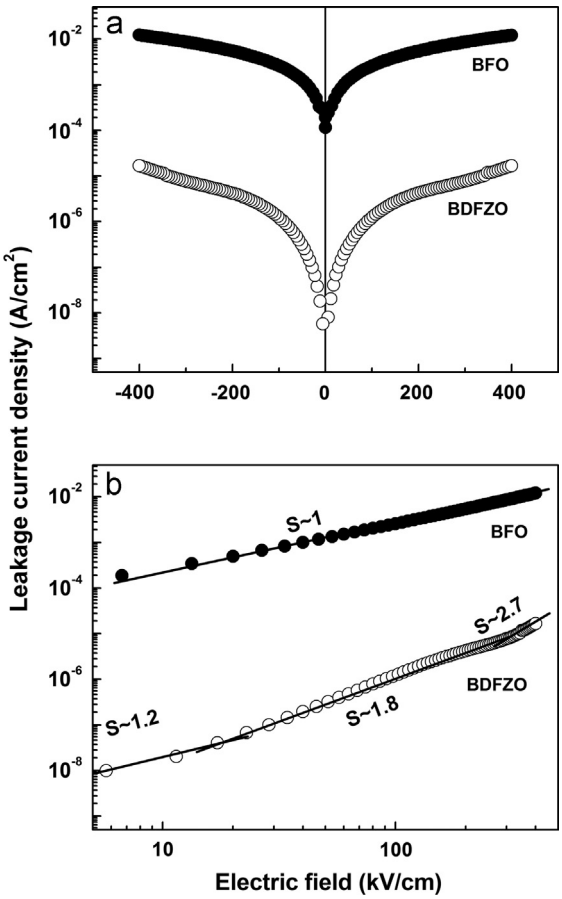


Fig. 4. (a) Leakage current densities of the BFO and the BDFZO thin films measured at room temperature and (b) log($J$)–log($E$) characteristics of each film showing the conduction mechanisms.

The leakage current mechanisms for the BFO and the BDFZO thin films were analyzed by the plots of log ($J$) versus log ($E$) as shown in Fig. 4(b). As shown in Fig. 4(b), the linearity of the line with the slope value $S \sim 1$ over the entire region of the applied electric field indicates Ohmic conduction mechanism for the BFO thin film [26]. Thermally generated electrons are mainly attributed to the Ohmic conduction in the BFO thin film. There are three linear segments with the $S$ values $\sim$1.2, $\sim$1.8 and $\sim$2.7 for the BDFZO thin film. At low electric field region the slope $\sim$1.2 indicates Ohmic conduction mechanism. The change of $S$ value from $\sim$1.2 to $\sim$1.8 with the increase of applied electric field indicates the change of conduction from Ohmic conduction to space charge limited (SCL) conduction mechanism [27]. At high electric field region, the density of free electrons due to carrier injection becomes greater than the density of thermally stimulated electrons. On further increasing of the electric field, the $S$ value becomes $\sim$2.7 which implies SCL conduction with other unknown mechanism [27]. From the leakage current analysis, the transport behavior of the BFO thin film is different from that of the BDFZO thin film.

The ferroelectric polarization–electric field ($P$–$E$) hysteresis loops of the BFO and the BDFZO thin films are shown in Fig. 5. The BDFZO thin films showed improved ferroelectric properties compared to the BFO thin film. The low remnant polarization ($2P_r$) of 35.1 μC/cm$^2$ and the large coercive field ($2E_c$) of 1360 kV/cm at an applied electric field of 1063 kV/cm were observed for the pure BFO thin film. While, the $2P_r$ and the $2E_c$ values of the BDFZO thin film were 47.0 μC/cm$^2$ and

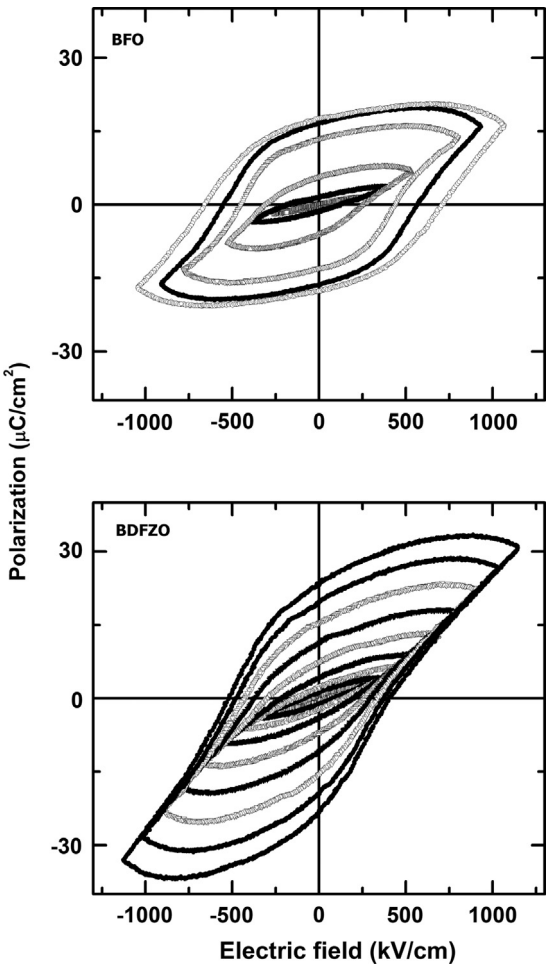


Fig. 5. Ferroelectric *P–E* hysteresis loops of the BFO and the BDFZO thin films measured at room temperature and a 10 kHz frequency.

925 kV/cm at an applied electric field of 1143 kV/cm, respectively. The improved ferroelectric properties, such as large remnant polarization and low coercive field of the BDFZO thin film, are correlated to the low leakage current density. The substitution of smaller ionic radius rare earth ions with higher electronegativity difference (relative to oxygen) for $Bi^{3+}$ dramatically strengthens the Bi(*RE*)–O covalent bond, which in turn induces a more pronounced off-center displacement along the [111] direction in the BFO thin films [10,23]. This should lead to an enhancement of ferroelectric properties of the BFO. Since, the ferroelectricity of the BFO mainly originated from the displacement of the $6s^2$ lone pair of $Bi^{3+}$ ion relative to oxygen atom. It has been reported that the ordering of the defect dipole is also significant to improve the polarization [17].

The dielectric properties of the thin films measured at room temperature in the frequency range from 100 Hz to 1 MHz are shown in Fig. 6. The dielectric constants of the thin films gradually decreased with increasing frequency. The dielectric constant and the dielectric loss values of the BFO and the BDFZO thin films were 61 and 0.053 and 83 and 0.035 at 1 kHz, respectively. Large dielectric constant and low dielectric loss for the co-doped BDFZO thin film are correlated with the low leakage current density of the thin film.

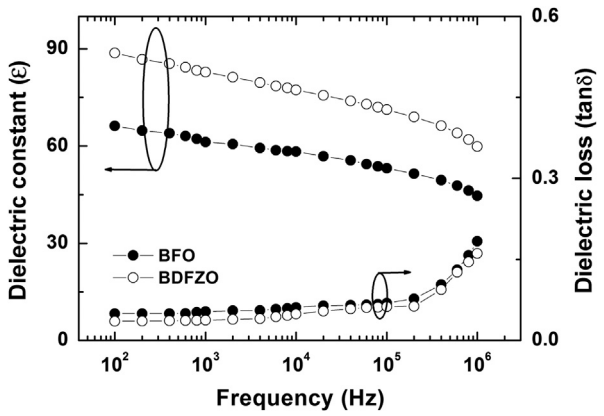


Fig. 6. Variations of dielectric constants and dielectric losses as functions of frequency of the BFO and the BDFZO thin films.

## 4. Conclusions

In summary, comparative studies were made on the pure $BiFeO_3$ (BFO) and the (Dy, Zn) co-doped $(Bi_{0.9}Dy_{0.1})(Fe_{0.975}Zn_{0.025})O_{3-\delta}$ (BDFZO) thin films prepared by the chemical solution deposition method. X-ray diffraction and Raman scattering studies showed more distortion in the rhombohedral lattices of the co-doped BDFZO thin film. The leakage current density of the BDFZO thin film was four orders lower than that of the pure BFO thin film. Reduced oxygen vacancies, formation of the defect dipole and smooth surface morphology were related to the low leakage current density of the BDFZO thin film. The enhanced ferroelectric properties of the co-doped BDFZO thin film are well correlated with its low leakage current density. The pronounced off-centered displacement and the defect dipole ordering in the perovskite structure might be attributed to the large polarization in the BDFZO thin film.

## Acknowledgment

This work was supported by Priority Research Centers Program through the National Research Foundation of Korea (NRF) funded by the Ministry of Education, Science and Technology (2010-0029634).

## References

[1] F. Zavaliche, S.Y. Yang, T. Zhao, Y.H. Chu, M.P. Cruz, C.B. Eom, R. Ramesh, Multiferroic $BiFeO_3$ films: domain structure and polarization dynamics, Phase Transitions 79 (2006) 991.
[2] G. Catalan, J.F. Scott, Physics and applications of bismuth ferrite, Advanced Materials 21 (2003) 2463.
[3] M.K. Singh, H.M. Jang, S. Ryu, M.H. Jo, Polarized Raman scattering of multiferroic $BiFeO_3$ epitaxial films with rhombohedral *R*3*c* symmetry, Applied Physics Letters 88 (2006) 042907.
[4] J.B. Neaton, C. Ederer, U.V. Waghmare, N.A. Spaldin, K.M. Rabe, First-principles study of spontaneous polarization in multiferroic $BiFeO_3$, Physical Review B 71 (2005) 014113.
[5] J. Wang, J.B. Neaton, H. Zheng, V. Nagarajan, S.B. Ogale, B. Liu, D. Viehland, V. Vaithyanathan, D.G. Schlom, U.V. Waghmare, N.A. Spaldin, K.M. Rabe, M. Wuttig, R. Ramesh, Epitaxial $BiFeO_3$ multiferroic thin film heterostructures, Science 299 (2003) 1719.

[6] X. Qi, J. Dho, R. Tomov, M.G. Blamire, J.L.M. Driscoll, Greatly reduced leakage current and conduction mechanism in aliovalent-ion-doped $BiFeO_3$, Applied Physics Letters 86 (2005) 062903.
[7] S.K. Singh, H. Ishiwara, K. Maruyama, Enhanced polarization and reduced leakage current in $BiFeO_3$ thin films fabricated by chemical solution deposition, Journal of Applied Physics 100 (2006) 064102.
[8] Z.X. Cheng, X.L. Wang, S.X. Dou, H. Kimura, K. Ozawa, Enhancement of ferroelectricity and ferromagnetism in rare earth element doped $BiFeO_3$, Journal of Applied Physics 104 (2008) 116109.
[9] I. Coondoo, N. Panwar, I. Bdikin, V.S. Puli, R.S. Katiyar, A.L. Kholkin, Structural, morphological and piezoresponse studies of Pr and Sc co-substituted $BiFeO_3$ ceramics, Journal of Physics D: Applied Physics 45 (2012) 055302.
[10] V.V. Lazenka, M. Lorenz, H. Modarresi, K. Brachwitz, P. Schwinkendorf, T. Böntgen, J. Vanacken, M. Ziese, M. Grundmann, V.V. Moshchalkov, Effect of rare-earth ion doping on the multiferroic properties of $BiFeO_3$ thin films grown epitaxially on $SrTiO_3$(100), Journal of Physics D: Applied Physics 46 (2013) 175006.
[11] S.K. Singh, K. Maruyama, H. Ishiwara, Reduced leakage current in La and Ni codoped $BiFeO_3$ thin films, Applied Physics Letters 91 (2007) 112913.
[12] G.L. Yuan, S.W. Or, H.L.W. Chan, Z.G. Liu, Reduced ferroelectric coercivity in multiferroic $Bi_{0.825}Nd_{0.175}FeO_3$ thin film, Journal of Applied Physics 101 (2007) 024106.
[13] T. Kawae, Y. Terauchi, H. Tsuda, M. Kumeda, A. Morimoto, Improved leakage and ferroelectric properties of Mn and Ti codoped $BiFeO_3$ thin films, Applied Physics Letters 94 (2009) 112904.
[14] Z. Hu, M. Li, Y. Yu, J. Liu, L. Pei, J. Wang, X. Liu, B. Yu, X. Zhao, Effects of Nd and high-valence Mn co-doping on the electrical and magnetic properties of multiferroic $BiFeO_3$ ceramics, Solid State Communications 150 (2010) 1088.
[15] C.M. Raghavan, J.W. Kim, S.S. Kim, Structural and electrical properties of chemical solution deposited $(Bi_{0.9}Tb_{0.1})(Fe_{0.975}\ TM_{0.025})O_{3\pm\delta}$ (TM=Ni, Mn and Ti) thin films, Journal of Sol–Gel Science and Technology 66 (2013) 168.
[16] K.G. Yang, Y.L. Zhang, S.H. Yang, B. Wang, Structural, electrical, and magnetic properties of multiferroic $Bi_{1-x}La_xFe_{1-y}Co_yO_3$ thin films, Journal of Applied Physics 107 (2010) 124109.
[17] G.D. Hu, S.H. Fan, C.H. Yang, W.B. Wu, Low leakage current and enhanced ferroelectric properties of Ti and Zn codoped $BiFeO_3$ thin film, Applied Physics Letters 92 (2008) 192905.
[18] S. Zhang, L. Wang, Y. Chen, D. Wang, Y. Yao, Y. Ma, Observation of room temperature saturated ferroelectric polarization in Dy substituted $BiFeO_3$ ceramics, Journal of Applied Physics 111 (2012) 074105.
[19] I.O. Troyanchuk, M.V. Bushinsky, D.V. Karpinsky, O.S. Mantytskaya, V.V. Fedotova, O.I. Prochnenko, Structural transformations and magnetic properties of $Bi_{1-x}Ln_xFeO_3$ (Ln=La, Nd, Eu) multiferroics, Physica Status Solidi B 246 (2009) 1901.
[20] F. Yan, M.O. Lai, L. Lu, T.J. Zhu, Enhanced multiferroic properties and valence effect of Ru-doped $BiFeO_3$ thin films, Journal of Physical Chemistry C 114 (2010) 6994.
[21] B. Yu, M. Li, J. Liu, D. Guo, L. Pei, X. Zhao, Effects of ion doping at different sites on electrical properties of multiferroic $BiFeO_3$ ceramics, Journal of Physics D: Applied Physics 41 (2008) 065003.
[22] P. Hermet, M. Goffinet, J. Kreisel, Ph. Ghosez, Raman and infrared spectra of multiferroic bismuth ferrite from first principles, Physical Review B 75 (2007) 220102.
[23] F. Yan, M.O. Lai, L. Lu, Domain structure and piezoelectric response in lanthanide rare earth-substituted multiferroic $BiFeO_3$ thin films, Journal of Physics D: Applied Physics 45 (2012) 325001.
[24] N. Jeon, D. Rout, I.W. Kim, S.J.L. Kang, Enhanced multiferroic properties of single-phase $BiFeO_3$ bulk ceramics by Ho doping, Applied Physics Letters 98 (2011) 072901.
[25] G.W. Pabst, L.W. Martin, Y.H. Chu, R. Ramesh, Leakage mechanisms in $BiFeO_3$ thin films, Applied Physics Letters 90 (2007) 072902.
[26] Q. Ke, X. Lou, Y. Wang, J. Wang, Oxygen-vacancy-related relaxation and scaling behaviors of $Bi_{0.9}La_{0.1}Fe_{0.98}Mg_{0.02}O_3$ ferroelectric thin films, Physical Review B 82 (2010) 024102.
[27] C. Wang, M. Takahashi, H. Fujino, X. Zhao, E. Kume, T. Horiuchi, S. Sakai, Leakage current of multiferroic $(Bi_{0.6}Tb_{0.3}La_{0.1})FeO_3$ thin films grown at various oxygen pressures by pulsed laser deposition and annealing effect, Journal of Applied Physics 99 (2006) 054104.